Progress In Electromagnetics Research M, Vol. 118, 163–175, 2023

Deep Flux Weakening Control of IPMSM Based on *D*-Axis Current Error Integral Regulator

Zhixuan Yi, Xiangfei Li*, Yang Yin, Junqin Liu, and Kaihui Zhao

Abstract—The deep flux weakening (FW) switching point of the interior permanent magnet synchronous motor (IPMSM) is difficult to track accurately. After entering the deep FW region, the current regulator is easily saturated, and the current following capability is poor. Aiming at these problems, a deep FW control of the IPMSM based on the d-axis current error integral regulator (DCEIR) is proposed. Firstly, the deep FW switching point is accurately calculated by using the maximum torque per volt (MPTV) as the limit of the d-axis current. Secondly, through the study of the voltage deviation, it is found that the q-axis regulating current is related to the DCEIR. On this basis, a new transformation relationship between d-axis current and q-axis current in the deep FW region is obtained. Finally, the simulation and experiment results are compared with the conventional negative d-axis current compensation method (NDCCM). It is verified that the proposed method can successfully restrain the saturation of the current regulator and enhance the current following capability in the deep FW region.

1. INTRODUCTION

Interior permanent magnet synchronous motors (IPMSMs) have permanent magnets located inside the rotor. The main inductance of the d-q axis is not equal. It can output reluctance torque and has stronger torque output capability than the surface-mounted permanent magnet synchronous motor (SPMSM). In addition, IPMSM can achieve speedup by weakening the d-axis magnetic flux, which can meet the needs of some high-speed applications.

After more than two decades of development, the control method of flux weakening (FW) control has gradually matured. The prevailing FW control methods are the formula method [1], table look-up method [2, 3], gradient descent method [4], leading angle FW control method [5, 6], and negative d-axis current compensation method (NDCCM) [7–12]. NDCCM is the most widely used FW control method, because it has a simple control method and high adaptability between different motors. However, at high speeds, the NDCCM is difficult to transfer the current trajectory from the shallow FW region to the deep FW region. Thus, other methods are needed to transfer the FW region to the deep FW region.

In [13], a mathematical model is constructed by rotational speed to determine the FW region at different speeds. However, the mathematical model depends on the parameters of the motor. When parameter perturbation occurs, the control effect is strongly influenced. In [14], a neural network algorithm was used to precisely find the deep FW switching point and achieve smooth switching from shallow FW control to deep FW control. However, the method requires a large amount of experimental data training. The constructed model is complicated. Ref. [15] used the gradient descent method to analyze the trend of torque and voltage changes. It determines the deep FW switching point by comparing the angular relationship of the torque change to the voltage limit ellipse, but the calculation steps are complicated and tedious. The computation is large. In [16], the conventional d-axis current

Received 1 August 2023, Accepted 22 August 2023, Scheduled 8 September 2023
* Corresponding author: Xiangfei Li (lixiangfei2006@163.com).
The authors are with the College of Electrical and Information Engineering, Hunan University of Technology, Zhuzhou 412007, China.

compensation is replaced by the q-axis current compensation. Smooth switching of different FW regions is achieved by comparing the magnitude of d-axis currents in different FW regions at the same q-axis current. Ref. [17] simplifies the calculation steps by approximating the maximum torque per volt (MTPV) control curve as a parabola. The approximated MPTV curve is used to accurately calculate the deep FW switching point. All of the above papers use different methods to achieve the switch from shallow FW region to deep FW region. However, the motor is highly susceptible to the loss of control after entering the deep FW region. The current needs to be distributed twice to avoid motor runaway in the deep FW region. How to distribute current reasonably in the deep FW region has become the focus of research.

When the current regulator is not saturated, the actual current follows the given current well. Therefore, the current error is close to zero. As the motor speed increases, the current regulator and inverter will gradually approach saturation. In the deep FW region, the current regulator is easily saturated, which makes the given current deviate greatly from the actual current. It reduces the stability of the system. In [18], a control strategy that can effectively avoid runaways is proposed by analyzing the principle of FW runaways. It directly uses the difference of the d-axis current to compensate the q-axis current. In [19], the transformation relationship between the q-axis regulating current and the difference of the d-axis current is obtained by derivation of the MPTV curve. But its calculation is complex and difficult to calculate in practical applications, and it is too dependent on the motor parameters. In order to make the calculation easier, literature [20] obtained the transformation relationship between q-axis current and d-axis current by taking the rotational speed increment from the voltage limit elliptic equation. It is simple to calculate and does not require multiple squares and square roots. However, in the deep FW region, it still leads to a large current deviation when the given current is too large.

This paper presents a deep FW control of IPMSM based on the d-axis current error integral regulator (DCEIR). Based on the NDCCM, it can accurately track deep FW switching points and improve current tracking capability and system stability in deep FW region.

2. MATHEMATICAL MODEL OF IPMSM

The stator voltage equation of IPMSM in the synchronous rotating d-q coordinate system is as follows:

$$\begin{cases} u_d = R_s i_d + \dfrac{d\psi_d}{dt} - \omega_e L_q i_q \\ u_q = R_s i_q + \dfrac{d\psi_q}{dt} + \omega_e (L_d i_d + \psi_f) \end{cases} \tag{1}$$

where u_d and u_q are the stator voltages in the d-axis and q-axis, respectively; i_d and i_q are the stator currents in the d-axis and q-axis, respectively; L_d and L_q are the stator inductances in the d-axis and q-axis, respectively; ω_e is the electric angular velocity; R_s is the stator resistance; and ψ_f is the permanent magnet flux linkage.

When the IPMSM is in steady-state operation, the approximate stator voltage equation can be obtained by ignoring the stator resistance:

$$\begin{cases} u_d \approx -\omega_e L_q i_q \\ u_q \approx \omega_e (L_d i_d + \psi_f) \end{cases} \tag{2}$$

When the motor is running, the stator current and stator voltage should satisfy the constraints:

$$\begin{cases} i_s = \sqrt{i_q^2 + i_d^2} \le i_{\lim} \\ u_s = \sqrt{u_q^2 + u_d^2} \le u_{\lim} \end{cases} \tag{3}$$

where i_s and u_s denote the stator current amplitude and voltage amplitude, respectively; $i_{\lim}$ and $u_{\lim}$ denote the maximum current and the maximum voltage that the inverter can sustain, respectively.

The voltage limit elliptic equation can be obtained by combining Eqs. (2) and (3):

$$\sqrt{(L_q i_q)^2 + (L_d i_d + \psi_f)^2} \le \frac{u_{\lim}}{\omega_e} \tag{4}$$

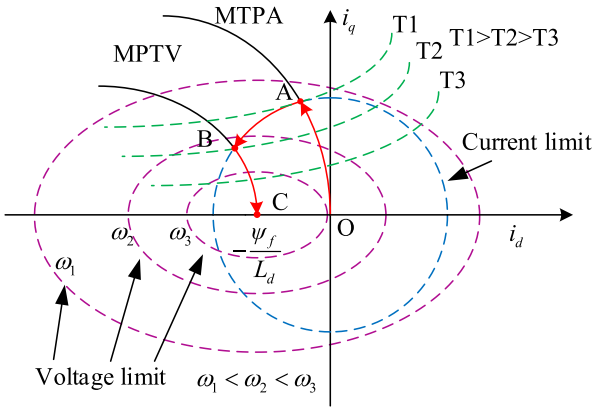

Figure 1. The current trajectory diagram of the FW control.

Figure 1 displays the current trajectory of the FW control. The IPMSM operation area consists of constant torque and constant power regions. The constant torque region is controlled by the maximum torque per ampere (MTPA). The constant power region consists of the shallow FW region and deep FW region. The shallow FW region is the area wrapped by the red curve as shown in Figure 1. It uses constant power control. The deep FW region is controlled by MPTV.

2.1. Maximum Torque Per Ampere (MTPA) Control

Below the rated speed, the current trajectory follows the MPTA curve. The MPTA trajectory is shown in the OA section of Figure 1. The stator current equation and electromagnetic torque equation can be obtained as:

$$\begin{cases} i_s = \sqrt{i_q^2 + i_d^2} \\ T_e = \dfrac{3}{2} n_p \left[\psi_f + (L_d - L_q) i_d\right] i_q \end{cases} \tag{5}$$

where T_e is the IPMSM electromagnetic torque, and n_p is the number of motor pole pairs.

Constructing the Lagrangian function from Eq. (5), the equation of the MPTA control can be obtained as:

$$\begin{cases} i_d = \dfrac{-\psi_f + \sqrt{\psi_f^2 + 4(L_d - L_q)^2 i_q^2}}{2(L_d - L_q)} \\ i_q = \sqrt{\dfrac{\psi_f i_d}{L_d - L_q} + i_d^2} \end{cases} \tag{6}$$

2.2. Maximum Torque Per Volt (MTPV) Control

Above the rated speed, the motor enters the shallow FW region. The current trajectory follows the current limiting circle in section AB of Figure 1. The motor reaches the deep FW region when the speed rises further. The current trajectory moves along the MPTV curve toward point C of Figure 1. The MPTV curve can be expressed as shown in section BC of Figure 1. The MPTV trajectory is shown in the BC segment in Figure 1. The solution equation can be obtained as:

$$\frac{\partial u_s}{\partial i_q} \cdot \frac{\partial T_e}{\partial i_d} - \frac{\partial u_s}{\partial i_d} \cdot \frac{\partial T_e}{\partial i_q} = 0 \tag{7}$$

From Eq. (2), the stator voltage follows as:

$$u_s^2 = (-\omega_e L_q i_q)^2 + (\omega_e L_d i_d + \omega_e \psi_f)^2 \tag{8}$$

Substituting Eqs. (5) and (8) into Eq. (7), the trajectory equation of MPTV can be obtained as:

$$i_d = -\frac{\psi_f}{L_d} + \frac{-L_q\psi_f + \sqrt{L_q^2\psi_f^2 + 4L_q^2(L_d - L_q)^2 i_q^2}}{2L_d(L_d - L_q)} \tag{9}$$

3. IPMSM DEEP FLUX WEAKENING RUNAWAY CAUSE ANALYSIS

Figure 2 shows the current trajectory of NDCCM. When performing FW control, the regulation direction of the NDCCM is fixed. It cannot be folded back. The current trajectory will move along the red curve in the A-B-D section as shown in Figure 2. Therefore, as the speed increases, the slope of the current trajectory continues to increase. It causes the q-axis current loop gain to become larger and larger, easily causing the current regulator to saturate. For this reason, it is necessary to appropriately limit the d-axis current, then bring it into MPTV control to avoid motor runaway.

The conventional NDCCM usually sets $i_{d\_set} = -\psi_f/L_d$ as the deep FW switching point. The current trajectory will move along the EC section curve in Figure 2. However, it results in a partial loss of speed regulation capability compared to the actual deep FW switching point, such as point B in Figure 2. Therefore, to increase the speed range of the motor, the actual deep FW switching point needs to be located.

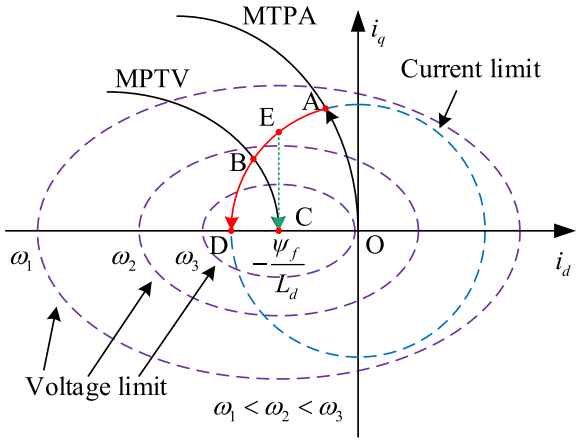

Figure 2. The current trajectory diagram of NDCCM.

4. DEEP FLUX WEAKENING CONTROL OPTIMIZATION STRATEGY

4.1. Negative *D*-Axis Current Compensation Method (NDCCM)

Above the rated speed, the output voltage goes beyond the maximum voltage output of the inverter ($u_{\lim} = u_{dc}/\sqrt{3}$). The inverter voltage output is saturated. The proportional-integral (PI) regulator of the voltage closed loop outputs the compensation value to decrease the d-axis current. The current trajectory will follow the current limit circle, and the current regulator avoids saturation. The compensation value can be expressed as:

$$\begin{cases} \sqrt{u_d^2 + u_q^2} \le u_{dc}/\sqrt{3}, & i_{dm} = 0 \\ \sqrt{u_d^2 + u_q^2} > u_{dc}/\sqrt{3}, & i_{dm} < 0 \end{cases} \tag{10}$$

where i_{dm} is the compensation output by PI.

4.2. Deep Flux Weakening Switching Strategy

The MPTV curve is used as the lower limit of the d-axis current. It makes the limit vary with the q-axis current. Figure 3 shows the current sizes of different curves under the same q-axis current. From Figure 3, at the same q-axis current, above point B, the d-axis current on the MPTV curve is significantly smaller than the d-axis current on the current limit circle. So the current is not limited. As the compensation is difficult to fold back below the B point, the current compensation will make the current trajectory continue to follow the current limit circle. The d-axis current value of the MPTV curve will be greater than the value on the current limit circle. Through the limiting effect of the MPTV curve, the current will switch to the MPTV curve. The difference in the d-axis current is as follows:

$$\Delta i_d = i_{do} + i_{dm} - i_{d\_set} \tag{11}$$

where Δi_d is the difference in the d-axis current, i_{do} the d-axis current output by MPTA, and i_{d_set} the limiting value output by MPTV.

The system determines the FW region in which the motor is running based on the difference in the d-axis current. When $\Delta i_d > 0$, it is running in the shallow FW region. When $\Delta i_d < 0$, it is running in the deep FW region. Therefore, the deep FW switching strategy can accurately track the deep FW switching point. Figure 4 shows the control block diagram of the deep FW switching strategy.

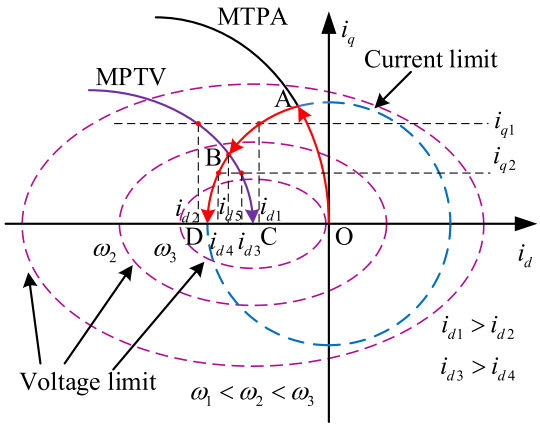

Figure 3. The current sizes of different curves under the same q-axis current.

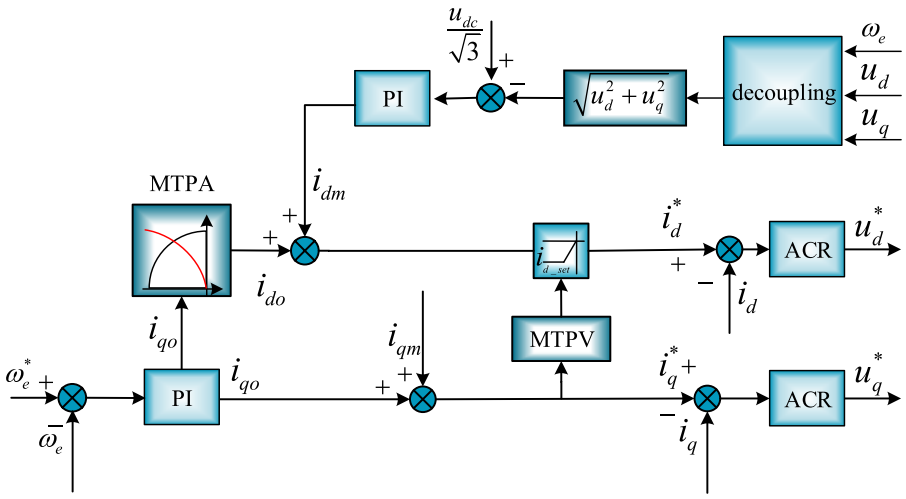

Figure 4. The block diagram of deep FW switching strategy control.

4.3. *D*-Axis Current Error Integral Regulator (DCEIR) Control Strategy

After entering the deep FW region, the d-axis current can no longer rise negatively. Thus, the secondary distribution of current at the deep FW region needs to be achieved by diminishing the q-axis current.

When the IPMSM is operating in the constant torque region, the voltage is inferior to the limit voltage of the inverter output. The error between the actual current and the system's given current is small. When the IPMSM is in the FW region, the inverter is saturated. The system-given voltage command deviates from the actual inverter output voltage. It makes the current error large. In the deep FW region, this phenomenon is especially obvious. Therefore, to improve the stability of IPMSM, the current regulator saturation needs to be suppressed.

From Eq. (2), the voltage deviation can be obtained as:

$$\begin{cases} \Delta u_d = u_d^* - u_d = u_d^* + \omega_e L_q i_q \\ \Delta u_q = u_q^* - u_q = u_q^* - \omega_e L_d i_d - \omega_e \psi_f \end{cases} \tag{12}$$

From Eq. (12), if we want to reduce the voltage deviation, we should take measures for the current.

The control system uses voltage feed forward decoupling. The given voltage can be expressed as:

$$\begin{cases} u_d^* = \left(K_p + \dfrac{K_i}{s}\right)(i_d^* - i_d) - \omega_e L_q i_q \\ u_q^* = \left(K_p + \dfrac{K_i}{s}\right)(i_q^* - i_q) + \omega_e L_d i_d + \omega_e \psi_f \end{cases} \tag{13}$$

Substituting Eq. (13) into Eq. (12) yields [21]:

$$\begin{cases} \Delta u_d = \left(K_p + \dfrac{K_i}{s}\right)(i_d^* - i_d) \\ \Delta u_q = \left(K_p + \dfrac{K_i}{s}\right)(i_q^* - i_q) \end{cases} \tag{14}$$

The direction of decreasing voltage error is represented by the gradient descent method. The voltage error change function can be expressed as:

$$F = \left(\Delta u_d^2 + \Delta u_q^2\right)/2 \tag{15}$$

Set the rate of change of the regulating current to be obtained as [22]:

$$\begin{pmatrix} \mathrm{d}i_{dm}/\mathrm{d}t \\ \mathrm{d}i_{qm}/\mathrm{d}t \end{pmatrix} = \alpha \nabla F \tag{16}$$

where i_{qm} is the q-axis regulating current; α is the modulation factor.

Integrate both sides of Eq. (16) and convert to the frequency domain, while taking the high-pass filter to filter out the direct current. The regulating current can be obtained as:

$$\begin{pmatrix} i_{dm} \\ i_{qm} \end{pmatrix} = \frac{\alpha}{s}\frac{s}{s+\omega_c}\nabla F = \frac{\alpha}{s+\omega_c}\begin{pmatrix} -\omega_e L_d \Delta u_q \\ \omega_e L_q \Delta u_d \end{pmatrix} \tag{17}$$

where ω_c is the filter cutoff frequency.

Substituting Eq. (14) into Eq. (17) yields:

$$i_{qm} = \frac{\alpha}{s+\omega_c}\omega_e L_q \left(K_p + \frac{K_i}{s}\right)(i_d^* - i_d) \tag{18}$$

Set the cutoff frequency $\omega_c = \frac{K_i}{K_p}$, modulation factor $\alpha = \frac{1}{\omega_e L_q}$, and substitute in Eq. (19) to be obtained as:

$$i_{qm} = \frac{K_p}{s}(i_d^* - i_d) \tag{19}$$

From Eq. (19), the q-axis regulating current is related to the DCEIR in the deep FW region. The current errors are inevitable during motor operation. In order to make i_{qm} only output in the deep FW

region, Δi_d is used to determine whether to output i_{qm}. When $\Delta i_d > 0$, the i_{qm} output is zero. When $\Delta i_d < 0$, the i_{qm} output is negative. Thus, i_{qm} should meet the following requirements:

$$\begin{cases} \Delta i_d > 0, & i_{qm} = 0 \\ \Delta i_d < 0, & i_{qm} < 0 \end{cases} \tag{20}$$

Because the current error is unavoidable, the value of the DCEIR changes all the time. When entering the deep FW control, the current will change greatly. It makes the FW region not smoothly switched, resulting in system instability. Therefore, a new q-axis regulating current needs to be redesigned.

The difference in d-axis current Δi_d is used as the criterion for determining the entry into the deep FW region. When the current entering the deep region, the difference in d-axis current is a continuous curve that starts from zero. In order to prevent sudden changes in the q-axis current when entering the deep FW region and to ensure the continuity of the current, the DCEIR is used as the relationship between the q-axis regulating current and the difference of the d-axis current. The relationship can be expressed as:

$$\frac{\Delta i_q}{\Delta i_d} = \frac{K_p}{s}(i_d^* - i_d) \tag{21}$$

where Δi_q is the new q-axis regulating current.

From Eq. (21), the new q-axis regulating current can be obtained as:

$$\Delta i_q = \frac{K_p}{s}(i_d^* - i_d) \cdot \Delta i_d \tag{22}$$

The expression for the given value of the current in the deep FW region can be obtained as:

$$\begin{cases} i_q^* = i_{qo} - \Delta i_q \\ i_d^* = -\dfrac{\psi_f}{L_d} + \dfrac{-L_q\psi_f + \sqrt{L_q^2\psi_f^2 + 4L_q^2(L_d - L_q)^2 i_q^2}}{2L_d(L_d - L_q)} \end{cases} \tag{23}$$

where i_{qo} is the q-axis given current output by MPTA.

The DCEIR control strategy has simple parameter adjustment and small calculation. It can effectively suppress the saturation of the current regulator and make the current have a good current dynamic following capability in the deep FW region. Figure 5 shows the IPMSM drive system.

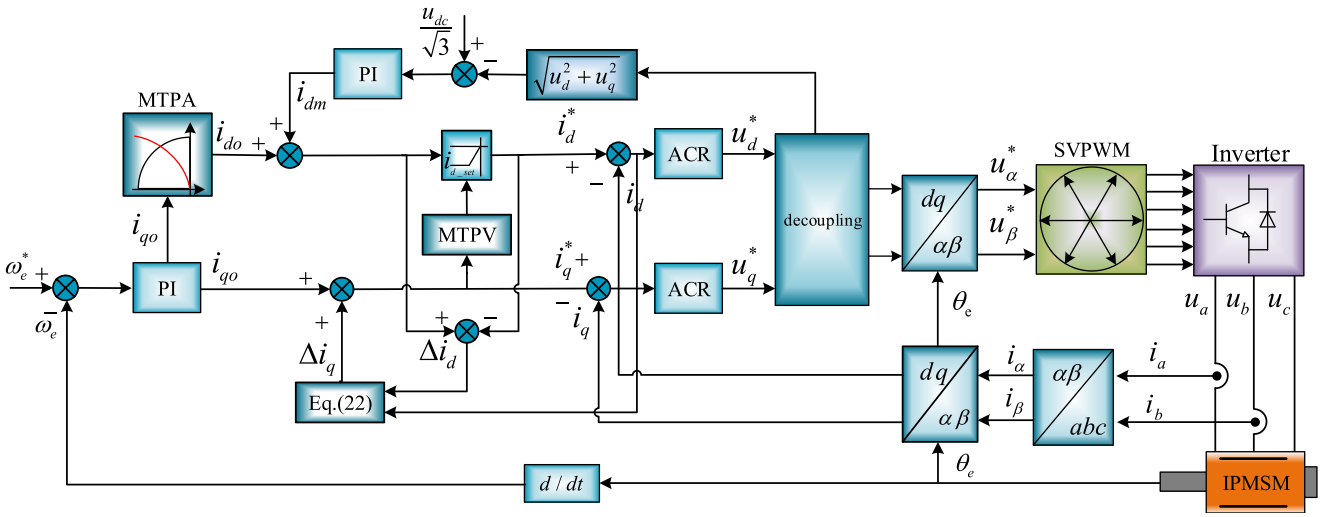

Figure 5. The block diagram of the IPMSM drive system.

5. ANALYSIS OF EXPERIMENTAL RESULTS

Through simulation and experiment, the viability and validity are verified by comparing the proposed method with the conventional negative d-axis current compensation method. Table 1 lists the parameters of the IPMSM.

Table 1. The parameters of IPMSM.

Parameters	Unit	Values
Dc voltage (u_{dc})	V	600
Rated speed (n_N)	r/min	1900
Q-axis inductance (L_q)	H	0.009
$D-$axis inductance (L_d)	H	0.004
Stator resistance (R_s)	Ω	2.75
Magnetic flux (ψ_f)	Wb	0.12
Viscous friction coefficient (B_m)	$\mathrm{N \cdot m \cdot s/rad}$	0.001
Inertia (J)	$\mathrm{kg \cdot m^2}$	0.029
Pole number (n_p)	pair	2

5.1. Simulation Result Analysis of IPMSM under Constant Speed Working Condition

The deep FW control strategy based on the DCEIR is compared with the conventional negative d-axis current compensation method by MATLAB/Simulink simulation. Both methods in the simulation use PI control. The simulation parameters are the same. Table 2 lists the parameters of the PI, automatic current regulator (ACR), and DCEIR.

Table 2. The parameters of control system.

Parameter	PI	D-axis ACR	Q-axis ACR	DCEIR
K_p	50	120	120	10
K_i	1000	200	300	/

At constant speed, the given speed is set as $n = 6000\,\mathrm{r/min}$. The load torque is set as $T_e = 14\,\mathrm{Nm}$. Figures 6(a), (b), (c), and (d) show the simulation results of speed, torque, and d-q axis current for the conventional NDCCM.

From the simulation results in Figure 6, the conventional NDCCM does not limit the d-axis current reasonably. It continues to follow the current limit circle after reaching the deep FW region. The q-axis current regulator gradually saturates. At 1.2 s, the pulsation of the q-axis current becomes larger, and the current begins to lose control. At 1.65 s, the q-axis current regulator has lost its ability to regulate. The current suddenly drops below zero. The stability of the motor decreases. The torque is also out of control along with the q-axis current. It drops below zero at 1.65 s. Thus, the speed starts dropping at 5430 r/min, which prevents the motor from reaching the given speed. Under the influence of the q-axis current, the d-axis current also shows a large change at 1.65 s. At 2.505 s, the speed drops to 200 r/min. The q-axis current regulator regains its regulating ability. The q-axis current, speed, and torque begin to rise. However, since the speed cannot reach the given speed. It will keep repeating the previous process.

Figures 7(a), (b), (c), (d), and (e) show the simulation results of speed, torque, d-q axis current, current trajectory, and d-axis current limit value variation for the deep FW control strategy based on the DCEIR.

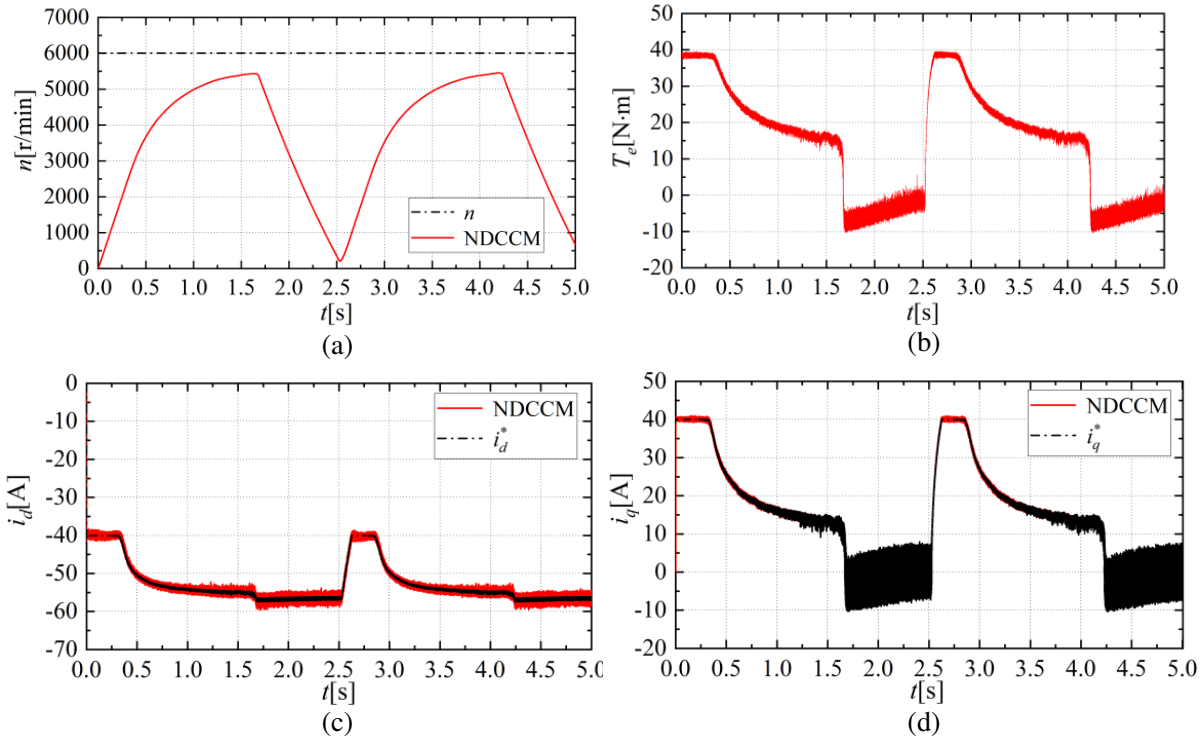

Figure 6. The simulation results of NDCCM. (a) Simulation results of speed. (b) Simulation results of torque. (c) Simulation results of d-axis current. (d) Simulation results of q-axis current.

From Figures 7(a) and (b), it can be seen that the speed rises steadily. The speed enters the steady state at 2.5 s and stabilizes at 6000 r/min. The motor enters the shallow FW zone at 0.3 s. The torque starts to decrease. Motor enters deep FW zone at 0.75 s. The torque is very smooth on switching in the FW region. The torque stabilizes at about 14 Nm at 1.8 s.

From Figures 7(c) and (d), the current is smooth during motor operation. At 0.3 s, the d-q axis current begins to decrease as it enters the shallow FW region. The d-axis current starts to ascend when it reaches -53 A. Then it enters the deep FW region. In the deep FW region, the current regulator is not saturated. The q-axis current is not out of control. The actual current follows the given current very well. At 2.0 s, the d-q axis currents stabilize at -25 A and 20 A, respectively.

From Figures 7(e) and (f), the MPTV curve and the d-axis given current intersect at -53 A. Therefore, the deep FW switching point is about -53 A. Then, the motor switches to the deep FW region. The d-axis current moves along the MPTV curve. The current trajectory is consistent with the theoretical trajectory of FW control. The feasibility and rationality of the deep FW switching strategy with MPTV as the d-axis current limit value are verified.

5.2. RT-LAB Experimental Analysis

Hardware-in-the-loop simulation (HILS) of the IPMSM was performed using the RT-LAB (OP5600) experimental platform to further validate the method. Figure 8 shows the experimental platform and system structure of RT-LAB. Figure 9 and Figure 10 show the experimental plots of the conventional NDCCM and the deep FW control strategy based on the DCEIR under the constant given speed condition, respectively. The experimental and simulation parameters are kept consistent.

The hardware-in-the-loop semi-physical system used in this paper adopts the structure of DSP controller and virtual controlled object to model the controlled object of the system, and the real-time simulator runs the solved model to interact with the real controller through the processing of the input and output signals of the simulator by the interface box, thus forming a semi-physical real-time simulation system. From Figure 8, RT-LAB (OP5600) is used to simulate the remaining components of

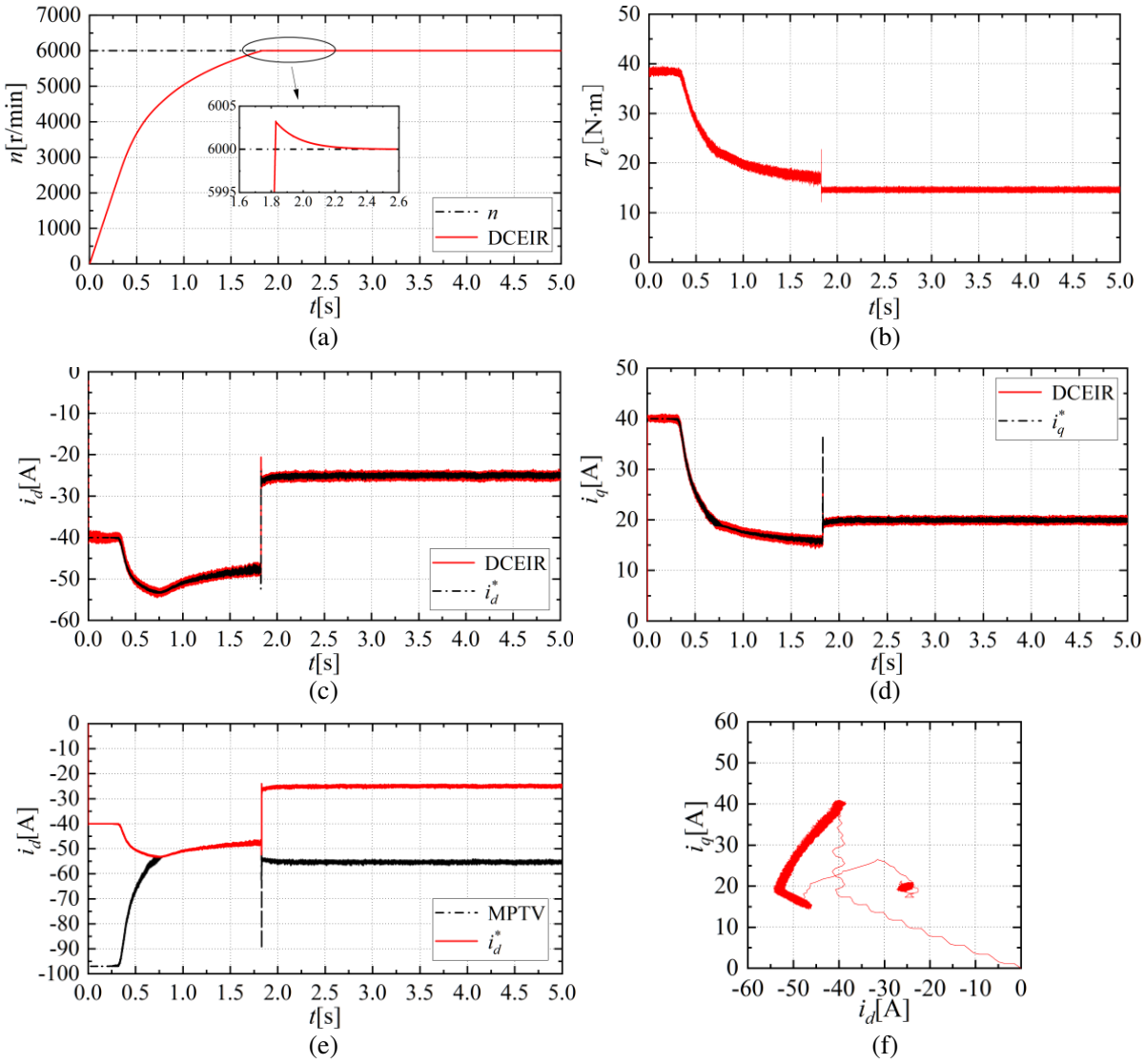

Figure 7. The simulation results of deep FW control based on DCEIR. (a) Simulation results of speed. (b) Simulation results of torque. (c) Simulation results of d-axis current. (d) Simulation results of q-axis current. (e) Simulation results of d-axis current limit value variation. (f) The current trajectory of FW control.

the motor system such as IPMSM and inverter. The model of the DSP controller is TMS320F2812. The hardware-in-the-loop semi-physical simulation platform experiments can be used to obtain experimental results consistent with the actual motor. The implementation of the control algorithm is mainly to build the algorithm model in the Simulink environment. Adjust the model to the best effect. Then download it into the RT-Lab controller and start running after ensuring that the platform parameters and indicators are normal. Transfer the experimental data to the oscilloscope to display the corresponding experimental results. Then analyze and study the real-time waveforms fed back from the monitoring interface to verify the feasibility of the control algorithm.

Compared with the simulation results in Figure 6 and Figure 7, the experimental precision is slightly degraded. The torque and current pulsations are larger. But the overall experimental trend is the same as the simulation. From Figure 9 and Figure 10, the conventional NDCCM is prone to be out of control in the deep FW region. The q-axis current regulator is saturated causing current runaway. However, the deep FW control strategy based on DCEIR can accurately switch to deep FW control. The current

trajectory moving along the MPTV curve can effectively suppresses the saturation of the q-axis current regulator. It makes the actual current follow the given current. The stability and speed range of the IPMSM drive system has been effectively improved.

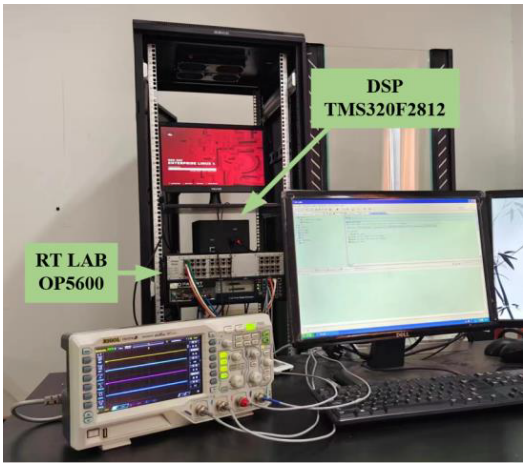

Figure 8. RT-Lab (OP5600) HILS experimental platform.

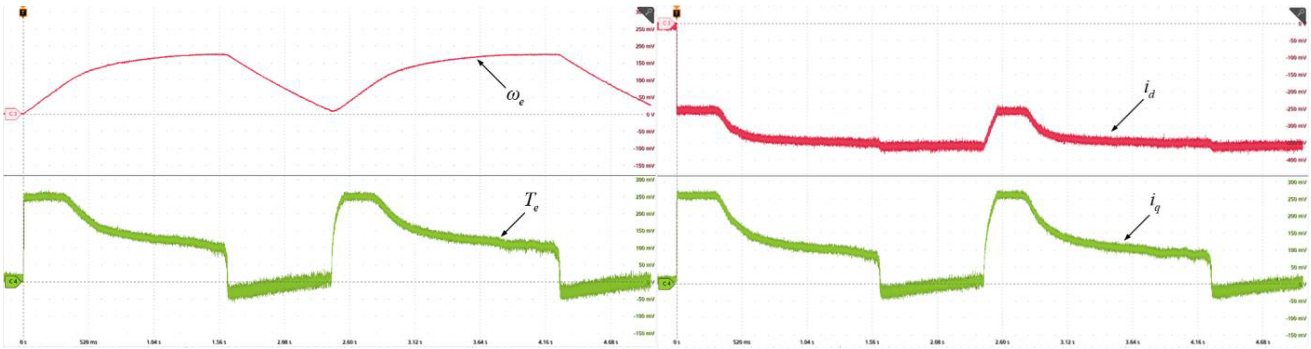

(a) (b)

Figure 9. The experimental results of NDCCM. (a) Experimental results of speed and torque. (b) Experimental results of d-q axis current.

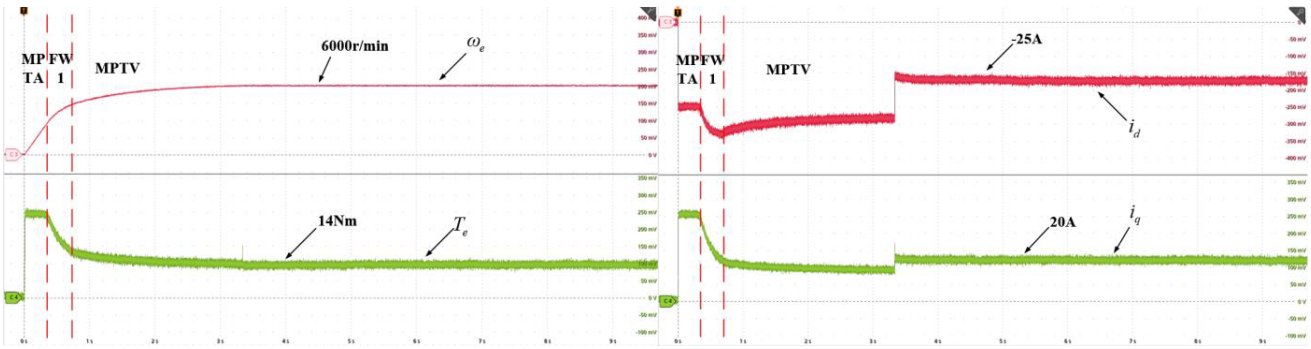

(a) (b)

Figure 10. The experimental results of deep FW control based on DCEIR. (a) Experimental results of speed and torque. (b) Experimental results of d-q axis current.

6. CONCLUSION

This paper presents a deep FW control strategy of the IPMSM based on the DCEIR. By using the MPTV curve as the limiting value of the d-axis current, the deep FW switching point is accurately tracked to achieve smooth switching from the shallow FW region to the deep FW region. A new current trajectory planning method in the deep FW region is proposed. It uses the DCEIR as the relationship between the q-axis regulating current and the difference of d-axis current to plan the current trajectory. The method has the advantages of being independent of the motor parameters, simple parameter adjustment, and small computational effort. By comparing the analysis results of the simulation and experiment with the conventional NDCCM at a given speed operating condition, the method can achieve smooth switching in the FW region, suppress the current regulator saturation, strengthen the current following ability in the deep FW region, and effectively improve the stability of IPMSM in the deep FW region.

ACKNOWLEDGMENT

This work was supported in part by Postgraduate Scientific Research Innovation Project of Hunan Province under Grant CX20231107 and in part by Project of Natural Science Foundation of Hunan Province under Grant 2023JJ50193.

REFERENCES

1. Zhang, X., Z. Zhao, and C. Xu, "A flux-weakening method for PMSM based model predictive direct speed control," *2020 IEEE 9th International Power Electronics and Motion Control Conference (IPEMC2020-ECCE Asia)*, 2557–2561, IEEE, 2020.
2. Yuniarto, M. N., I. Sidharta, Y. Yohanes, et al., "On the development and experimental validation of a novel and intuitive interior permanent magnet synchronous motor controller for electric vehicle application," *World Electric Vehicle Journal*, Vol. 13, No. 6, 107, 2022.
3. Tan, B., H. Chen, X. Li, et al., "Torque-current lookup table establishment method for PMSM considering parameter nonlinear characteristics," *2022 25th International Conference on Electrical Machines and Systems (ICEMS)*, 1–6, IEEE, 2022.
4. Qian, X., X. Guo, H. Qin, et al., "Research on the application of flux-weakening control in PMSM with wide range speed variation," *2017 International Conference on Smart Grid and Electrical Automation (ICSGEA)*, 371–374, IEEE, 2017.
5. Miguel-Espinar, C., D. Heredero-Peris, G. Gross, et al., "Maximum torque per voltage flux-weakening strategy with speed limiter for PMSM drives," *IEEE Transactions on Industrial Electronics*, Vol. 68, No. 10, 9254–9264, 2020.
6. Pan, Y., X. Liu, Y. Zhu, and Z. Li, "A leading angle flux weakening control method for PMSM based on active disturbance rejection control," *Progress In Electromagnetics Research C*, Vol. 121, 29–38, 2022.
7. Xu, Y., W. Zhang, and D. Sun, "Comparative research of two flux-weakening method of PMSMs in high speed range," *2017 20th International Conference on Electrical Machines and Systems (ICEMS)*, 1–5, IEEE, 2017.
8. Lee, H., G. Lee, G. Kim, et al., "Variable incremental controller of permanent-magnet synchronous motor for voltage-based flux-weakening control," *Energies*, Vol. 15, No. 15, 5733, 2022.
9. Zheng, X., Y. Xi, L. Zhang, et al., "Review of flux weakening control methods of permanent magnet synchronous motor," *Automation Application*, Vol. 12, 1–3+6, 2019, doi: 10.19769/j.zdhy.2019.12.001.
10. Liu, Y., X. Wu, and Q. Li, "Permanent magnet synchronous motor nonlinear regulator MTPA flux weakening control," *Mechanical and Electrical Information*, Vol. 1, 11–15, 2023, doi: 10.19514/j.cnki.cn32-1628/tm.2023.01.004.
11. Sepulchre, L., M. Fadel, M. Pietrzak-David, et al., "New high speed PMSM flux-weakening strategy," *2016 19th International Conference on Electrical Machines and Systems (ICEMS)*, 1–6, IEEE, 2016.

12. Li, S., J. Su, and G. Yang, "Flux weakening control strategy of permanent magnet synchronous motor based on active disturbance rejection control," *Journal of Electrotechnics*, Vol. 37, No. 23, 6135–6144, 2022, doi: 10.19595/j.cnki.1000-6753.tces.211129.
13. Lutonin, A., A. Shklyarskiy, and Y. Shklyarskiy, "Operation modes and control algorithms of anisotropic permanent magnet synchronous motor (IPMSM)," *E3S Web of Conferences*, Vol. 140, 10006, 2019.
14. Dong, W., S. Li, Y. Gao, et al., "Neural network with cloud-based training for MTPA, flux-weakening and MTPV control of IPM motors and drives," *IEEE Transactions on Transportation Electrification*, IEEE, 2023.
15. Wang, J., C. Ren, Z. Liu, et al., "Research on direct drive technology of the permanent magnet synchronous motor for urban rail vehicles," *Mathematical Problems in Engineering*, 2022.
16. Cao, C., Z. Lan, F. Shen, et al., "Deep flux weakening control of interior permanent magnet synchronous motor based on quadrature-axis current compensation," *Micromotors*, Vol. 55, No. 1, 63–70, 2022, doi: 10.15934/j.cnki.micromotors.2022.01.009.
17. Xiao, R., S. Peng, and Z. Huang, "A novel deep flux weakening control strategy for IPMSM," *The Proceedings of the 16th Annual Conference of China Electrotechnical Society: Volume II*, 279–290, Springer Nature, Singapore, 2022.
18. Zhu, L., X. Wen, F. Zhao, et al., "Control policies to prevent PMSMs from losing control under field-weakening operation," *Proceedings of the CSEE*, Vol. 31, No. 18, 67–72, 2011, doi: 10.13334/j.0258-8013.pcsee.2011.18.012.
19. Shi, W. and X. Jin, "A permanent magnet synchronous motor q-axis current error integral feedback depth field-weakening control strategy," *Electric Machines and Control Applications*, Vol. 45, No. 7, 23–29, 2018.
20. Zhu, L., X. Wang, and H. Zhu, "An IPMSM deep flux weakening algorithm with calculable parameters to avoid out-of-control," *Proceedings of the CSEE*, Vol. 40, No. 10, 3328–3336, 2020, doi: 10.13334/j.0258-8013.pcsee.190945.
21. Zhou, H., L. Chen, G. Liu, et al., "Flux-weakening strategy for improving PMSM dynamic performance," *Electric Machines and Control*, Vol. 18, No. 9, 23–29, 2014, doi: 10.15938/j.emc.2014.09.022.
22. Wang, A., X. Jia, and L. Zhang, "A new flux-weakening control strategy considering voltage saturation for IPMSM drives," *Proceedings of the 31st Chinese Control Conference*, 4295–4299, IEEE, 2012.